

## High Visible Response of Vertical TiO<sub>2</sub> Nanoclusters-CdSe Linked by Cysteine†

FU FANG ZHOU<sup>1,2</sup>, DELONG LI<sup>1</sup>, WENHUI WU<sup>1</sup>, LIUYING ZHAO<sup>2</sup>, PING WANG<sup>3</sup>, YUAN MING HUANG<sup>4,\*</sup> and CHUNXU PAN<sup>1,\*</sup>

<sup>1</sup>School of Physics and Technology and MOE Key Laboratory of Artificial Micro- and Nano-structures, Wuhan University, Wuhan 430072, P.R. China

<sup>2</sup>College of Physics & Electronic Information, Yunnan Normal University, Kunming 650500, P.R. China

<sup>3</sup>College of Chemistry & Chemical Industry, Yunnan Normal University, Kunming 650500, P.R. China

<sup>4</sup>School of Mathematics and Physics, Changzhou University, Jiangsu 213164, P.R. China

\*Corresponding authors: E-mail: [dongshanisland@126.com](mailto:dongshanisland@126.com); [cspan@whu.edu.cn](mailto:cspan@whu.edu.cn)

AJC-15743

Vertically oriented single-crystal TiO<sub>2</sub> nanoclusters in tetramethylammonium hydroxide solution were synthesized hydrothermally directly on Ti substrate. N-Type semiconducting CdSe nanoparticles were then introduced deep coating TiO<sub>2</sub> nanocrystals *via* a two-step procedure using cysteine as a surface coupling agent, followed by a subsequent electrodeposition process from selenosulfite to form orderly interconnecting heterojunctions. A key result achievement is that although the TiO<sub>2</sub> nanocrystals are less than 1 μm long, under the help of the bifunctional 2-amino-3-sulfhydrylpropanoic acid molecule linking the acceptor and donor materials, the virtue of strong visible absorption of single crystal TiO<sub>2</sub> nanoclusters were fully developed in addition of ultraviolet, so that the heterojunction electrode exhibits excellent photoresponse in photoelectrochemical cells to visible lights, whose contribution is rather significant compared with that of ultraviolet lights. Vertical nanoclusters have advantages of leading electrons directly into the metal Ti substrate while maintaining the large surface area towards the electrolyte. These highly ordered nanohybrids are expected to have potential applications in photochemical solar cells with high efficiency.

**Keywords:** TiO<sub>2</sub> nanocluster, CdSe, Vertically oriented, Visible lights, Sensitization.

### INTRODUCTION

Highly ordered semiconductor materials are suitable for solar cell electrode fabrication<sup>1-4</sup>. Well-ordered nanostructures allow maximal excitons (photogenerated bound electron-hole pairs) to reach semiconductor interface and maximal charge carriers to reach corresponding electrode *via* rapid pathways. Therefore, highly ordered semiconductor is very important for inorganic, polymer and hybrid solar cells, according to the semiconductor heterojunction photovoltaic mechanism<sup>1-4</sup>.

Titanium(IV) dioxide is an important semiconductor material for easy one dimensional (1D) nanomaterial fabrication, including nanowires and nanotubes. These materials can be used for not only key semiconductor phases but also skeleton to support sensitizer such as quantum dots (QDs) or soft polymer “muscles” suitable for photocatalysis and solar cells as QD-, polymer- and dye-sensitized solar cells (DSSC), respectively<sup>5-8</sup>. The performance of TiO<sub>2</sub> is strongly dependent on its phase structure, morphology and other properties<sup>9-14</sup>.

1D TiO<sub>2</sub> features direct pathways for photogenerated electrons, which outperform percolation paths<sup>15</sup>. Single crystalline 1D TiO<sub>2</sub> has aroused intensive research interest in solar cell field. It inspires the expectation superior photovoltaic performance including 1) a fine nanoscale intermixing<sup>1</sup> with high exciton separation 2) “bidirection-highway” transportation for inverse sign of charge carriers and 3) long minority carrier lifetime<sup>1,2,16-22</sup>. Vertically aligned 1D nanostructure excels disorderly oriented 1D nanostructure in DSSC performance due to increased charge-collection probability<sup>16-18,23</sup>. If single crystalline TiO<sub>2</sub> can even be constructed upon Ti foil substrate to form ohmic contact, higher efficiency can be exploited, but has achieved high photocurrent density under visible light remembering similar ohmic contact of ZnO/Ti<sup>24</sup>.

Quantum dot sensitized solar cell is interesting due to its tunable energy gap related to particle size, broad spectral response [from ultraviolet (UV) to the near infrared (IR)] and long exciton lifetimes. More interestingly, the properties of multiple exciton generation (MEG) and hot carrier

†Presented at 2014 Global Conference on Polymer and Composite Materials (PCM2014) held on 27-29 May 2014, Ningbo, P.R. China

extraction minimize the loss of high energy carriers. However, only modest multiple exciton generation process efficiency was reported. And the lack of hot electron injection and slow electron transfer rate are the primary reasons for slow electron transfer time<sup>25-28</sup>. Only recently, hot carrier and multiple exciton extraction from QD to TiO<sub>2</sub> single crystals have been realized<sup>29</sup>. The electrons undergo ultrafast propagation into the TiO<sub>2</sub> conduction band due to the strong mixing of QD and TiO<sub>2</sub> electronic levels<sup>29</sup>. It is notable that TiO<sub>2</sub> single crystals are often chosen as optimal phase to couple with QD to test the multiple exciton generation effect, primarily due to its high transportation rate of electrons and thus high inhibition of electron-hole recombination.

In this work, our purpose was to incorporate CdSe into vertical TiO<sub>2</sub> single crystal nanoclusters to examine the effect on photoelectrochemical performance. Although beneficial, it is difficult to induce CdSe deep into the TiO<sub>2</sub> nanostructure forest, so a pre-treatment on the surface of TiO<sub>2</sub> single crystal nanoclusters was designed. We used cysteine (2-amino-3-sulfhydrylpropanoic acid) as a surface coupling agent, followed by a subsequent potentiostatic electrodeposition process from selenosulfite to form the nanoscale orderly and closely coated CdSe-TiO<sub>2</sub> interconnecting heterojunctions. Characterizations were performed, including surface morphologies, material structure analysis (XRD), UV-visible absorption, photoresponse towards on-off UV as well as visible lights, dependence of current on potential. Interestingly, as the result of closely interpenetrating CdSe into host phases and directly oriented to collection electrodes, the obtained Ti/TiO<sub>2</sub>/CdSe nanoclusters electrode showed superior photoelectric conversion towards polysulfide reduction in terms of photocurrent response. Consequently, vertical orientation is an important and indispensable fact for its excellent performance in solar cells.

## EXPERIMENTAL

The synthesis method of titanium (TiO<sub>2</sub>) is described by Zhang and Banfield<sup>30</sup>. A titanium plate (99.99 % purity) with a size of 3.0 cm × 2.0 cm × 0.1 mm was rinsed by distilled water and dried in the oven. The sample was then immersed in 30 mL 0.5 M tetramethylammonium hydroxide solution contained in a 100 mL Teflon-lined stainless steel autoclave. The autoclave was heated to 200 °C for various durations in the oven. After the hydro-thermal treatment, the sample was thoroughly rinsed with distilled water for several times before being dried in the oven at 70 °C.

The morphology of the sample was observed using field emission scanning electron microscopy (FESEM, FEI SIRION, The Netherlands), with attached energy-dispersive X-ray spectrometer, EDS. The X-ray diffraction (XRD) measurement was performed using a Bruker D8 diffractometer with CuK<sub>α</sub> with radiation being operated at 40 kV and 40 mA ( $\lambda = 0.154056$  nm). The UV-visible absorbance spectra of the samples were measured using a UV-visible spectrophotometer (SHIMADZU UV-2550, 0.5 nm resolution) in combination with diffuse reflectance integrator accessory and with BaSO<sub>4</sub> as the background.

5 mM Na<sub>2</sub>SeSO<sub>3</sub> solution was prepared by mixing 0.1 M Na<sub>2</sub>SO<sub>3</sub> and weighed powdered 5 mM Se in 1M NH<sub>3</sub>/NH<sub>4</sub><sup>+</sup> buffer in a 70 °C bath until Se was completely dissolved. All solutions were prepared with triply distilled water and reagent grade of Na<sub>2</sub>SO<sub>3</sub>, NH<sub>4</sub>OH, NH<sub>4</sub>Cl, CdSO<sub>4</sub> and ethylene diamine tetraacetic acid (EDTA) Na<sub>2</sub> with a concentration of 0.1, 1, 1, 0.2 and 0.2 M, respectively. The pH value was measured to be about 10<sup>31</sup>.

All CdSe thin films were electrodeposited on TiO<sub>2</sub> substrates. Standard CdSe deposition on TiO<sub>2</sub> was carried out potentiostatically at various potentials. A standard three electrode configuration was used with Ti/TiO<sub>2</sub> substrate as the working electrode on a polyfuron set, a saturated calomel as the reference electrode and Pt as the counter electrode. A new solution was made for each deposition. But for TiO<sub>2</sub>(II), the process was different in that Ti/TiO<sub>2</sub> substrates were immersed in 0.1 M 2-amino-3-sulfhydrylpropanoic acid aqueous solution for 6 h at room temperature in advance of CdSe deposition.

Photoelectrochemical measurements were carried out on an electrochemical workstation (CHI660D, Shanghai Chenhua Instrument Co., Ltd., Shanghai, China). A 150 W Xe lamp (CHF-XM-500W, Beijing Changtuo Co. Ltd., Beijing, China) equipped with an AM 1.5G filter was used as the light source. The intensity of the incident light was measured with solar power meter TES 1333 (TES Co., Taiwan China) and fixed at 100 mW cm<sup>-2</sup> under air mass 1.5 global (AM 1.5 G, using 1.5 AM filter, Beijing Changtuo Co. Ltd., Beijing, China). A 410 nm long pass filter was used to remove light with wavelength less than 410 nm and resulting in an ultimate visible light with an intensity of 80.4 mW cm<sup>-2</sup>. Similarly, a 410 nm short pass filter was used to obtain light with wavelength less than 410 nm, resulting in an ultimate UV light with an intensity of 19.6 mW cm<sup>-2</sup>. The current density *versus* potential (J-V) curve of the working electrode was measured by a linear sweep voltammogram with a potentiostat CHI660D. In all J-V measurements, a two-electrode configuration similar to that typically used for solar cells test was used. Photoelectrode Ti/TiO<sub>2</sub>/CdSe was the working electrode and Pt was as the counter electrode. A scan rate of 20 mV/s was used for the linear sweep voltammogram. The photoresponse of the different samples were characterized by potentiostatic (current vs time, I-t) measurements under intermittent illumination at zero bias *versus* saturated SCE electrode by front-wall (through the electrolyte) illumination mode. Before any photocurrent measurement, the edge of a CdSe-sensitized TiO<sub>2</sub> photoanode was sealed with epoxy resin. Photocurrent response to on-off illumination at zero bias *versus* saturated SCE electrode was measured electrochemically in a standard three-electrode configuration. A polysulfide redox electrolyte was prepared using 1 M Na<sub>2</sub>S, 1 M S and 1 M NaOH in an aqueous solution. The active area of the cell in polysulfide electrolyte under illumination is 0.1 cm<sup>2</sup>.

## RESULTS AND DISCUSSION

Fig. 1 shows the FESEM images of the nanoclusters unprepared and synthesised in 200 °C for 6 h and 12 h, respectively. In Fig. 1(a), featureless flat surface was observed on as purchased pure Ti foils. Overall network of "thorns" termed as TiO<sub>2</sub> (I) in (b) can be observed, (c) and (d) show the top-

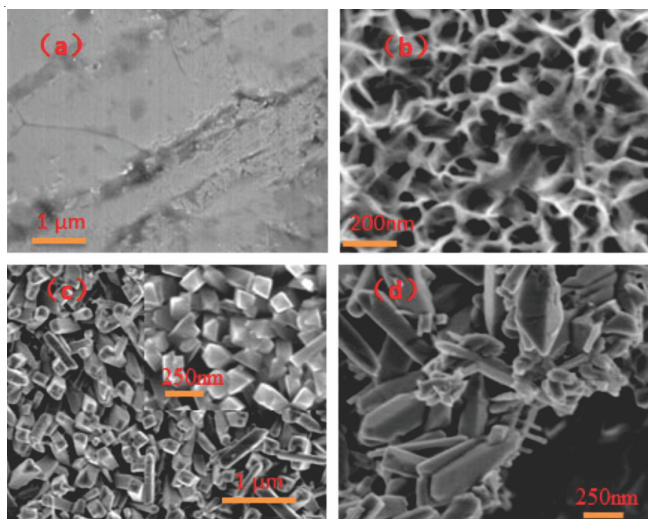


Fig. 1. FESEM images of Ti before hydrothermal synthesis as the substrate and building blocks for TiO<sub>2</sub> nano architectures (a); TiO<sub>2</sub> architecture (I) synthesized for 6 h at 200 °C (b); TiO<sub>2</sub> architecture(II) synthesized for 12 h at 200 °C with the top-view of the nano-pillars arrays (c), the side-view of the piled-up nano-pillars showing the bottom of the pillars near substrate (d), respectively

view and side-view of the synthesized architecture termed as TiO<sub>2</sub>(II). In (c), numerous nanoclusters stand upright and the pillar tips were flat with bipyramid shape. According to the calculations by Wu *et al.*<sup>32</sup>, the bipyramid rod-like shape is more stable than other shapes. The diameter ranges from a few tens of nanometers to around 300 nm, with an average of less than 100 nm. Despite the width variation, the length of pillars are almost constant at 500-600 nm. This suggests that the growth of long nanoclusters starts and ends at the same time. And wider pillars might originate from the mержence of thinner ones, which is a typical phenomenon of nanopillars or nanorods bundle concerning precursor concentration<sup>7</sup>. Nevertheless, at the bottom of the pillars, there exist some smaller shoots without a uniform morphology and orientation which are less crystallized. For ellipsoids-like TiO<sub>2</sub> crystals growth on the surface of Ti plate with the aid of the selective absorption of TMA units and amine groups under hydrothermal condition, the continuous repetition of these steps induces the final TiO<sub>2</sub> nano-pillars. When the length of nanopillars increases at the top in the hydrothermal reaction area, the bottom zone might suffer from insufficient reaction reagents, thus suppressing the growth to full length<sup>32</sup>. The growth mechanism for TiO<sub>2</sub> might be explained as follows. The lattice planes parallel to (0 0 1) of anatase TiO<sub>2</sub> act as assembling templates while TMA and amine group selectively adsorb onto them by H-bonding TMA units stack layer by layer, the growth of the crystal planes choose to become parallel to c-axis, suppressing the direction perpendicular to c-axis<sup>33,34</sup>.

Fig. 2 shows the XRD patterns of the TiO<sub>2</sub> (I) (for 6 h) and TiO<sub>2</sub> (II) (for 12 h) synthesized hydrothermally in 0.5 M in newly prepared solution at 200 °C, respectively. Ti foil before synthesis was used as the reference. On the up left corner, JCPDS card numbers for anatase, rutile and Titanium are denoted as 21-1272, 79-1640 and 44-1294, respectively. Only peaks of Ti were observed in samples of as received pure Ti foils. However, the orientation preference of Ti is prominent, as the

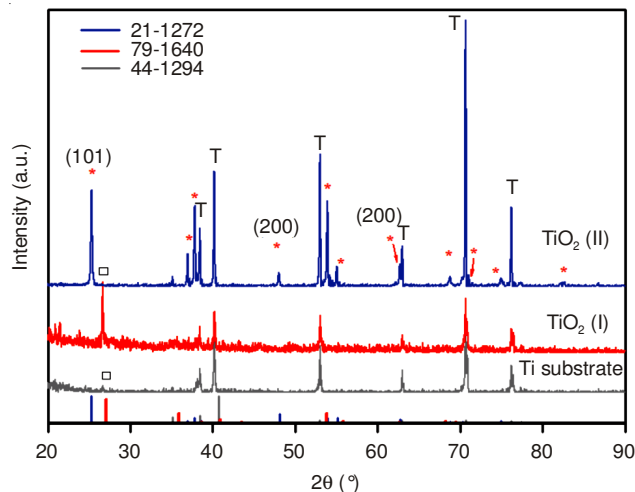


Fig. 2. XRD patterns of TiO<sub>2</sub> (I), TiO<sub>2</sub> (II) films with 6 and 12 h of hydrothermal growth in tetramethylammonium hydroxide (TMAOH), in comparison with Ti substrate

diffraction peak of 27.2° (JCPDS No. 44-1294) is missing. The peaks in Ti also dominate in TiO<sub>2</sub> (I) and the only strong peak different from Ti substrate is well indexed to TiO<sub>2</sub> rutile (JCPDS No. 79-1640), suggesting the nano architectures TiO<sub>2</sub> (I) might be rutile. Some distinct peaks appear besides the peaks ascribed to Ti in TiO<sub>2</sub> (II) patterns well indexed to the standard anatase phase (JCPDS No. 21-1272), suggesting the anatase phase was well defined.

Fig. 3(a-d) presents FESEM images of CdSe deposited at -1.33 V to -1.24 V potentiostat on TiO<sub>2</sub> (I), respectively. The more negative deposition potential, the smoother morphology, the more homogeneous. Until image (d), obvious phase separation can be observed and the heterogeneous surface is littered with clusters as large as 250 nm. Fig. 3 (e) and (f) presents CdSe deposited potentiostatically at -1.33 V for 100 and 200 s, respectively on TiO<sub>2</sub>(II) nano-clusters, after a 6 h immersion in 2-amino-3-sulfhydrylpropanoic acid. In (e), CdSe critically change the morphology represented in Fig. 1 (c) and (d), for numerous CdSe nano particles deeply inserting the interspace between nanoclusters, as well on top end of nanoclusters. In Fig. 3(f) CdSe completely change the morphology represented in Fig. 1(c) and (d). EDS analysis reports the atomic composition ratios of Cd:Se in (a) to (f) are 1.08, 1.13, 0.85, 0.57, 0.88 and 1.11, respectively, suggesting that the coarse agglomerate in (d) might be excessive Se. Typical EDS results are also illustrated in Fig. 3(g) corresponding to above (a) -1.33V, 10s CdSe/TiO<sub>2</sub> (I) and (f) -1.33V, 200s CdSe/TiO<sub>2</sub> (II), respectively. The ratio tendency of Cd:Se from (a) to (d) with the varying potential is reasonable, considering the cathodic electro-deposition method we employed, the more negative the the cathodic potential the more concentration of cations in the solution are attracted to the work electrode TiO<sub>2</sub>.

Fig. 4 shows UV/visible spectra of TiO<sub>2</sub> (I), CdSe-TiO<sub>2</sub> (II), 200 s potentiostatic CdSe deposition on TiO<sub>2</sub> (I) and TiO<sub>2</sub> (II). Utterly different from general TiO<sub>2</sub> nanotube or nanowire, there are wide and strong absorption bands in visible range. There are yet a minimum separation between UV and visible bands in bare TiO<sub>2</sub> (I) and TiO<sub>2</sub> (II), but the separation disappears when incorporating with CdSe. According to the reference<sup>35</sup>, the visible absorption broad band might be the oxygen

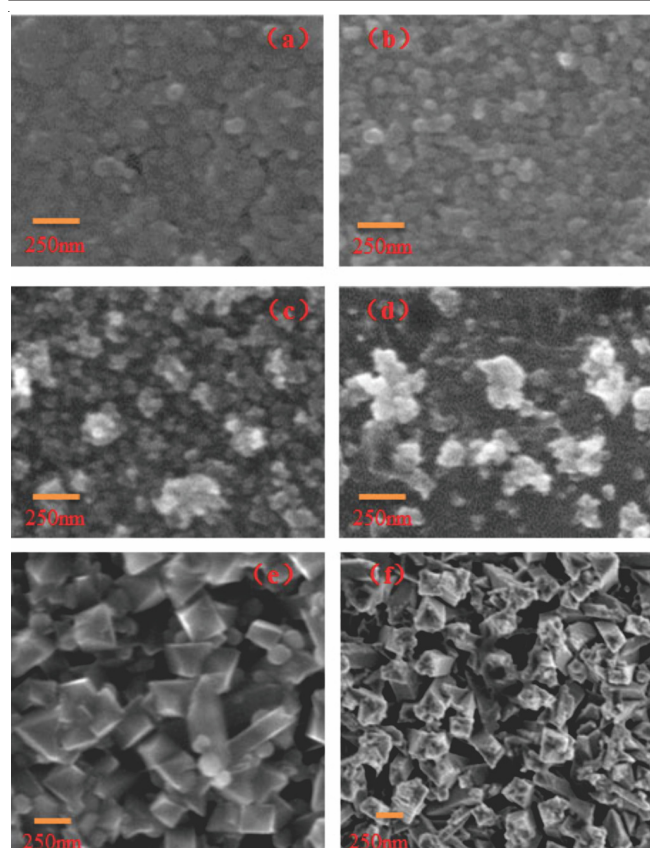


Fig. 3. FESEM images of CdSe deposited potentiostatically for 200s at -1.33V (a); -1.30V (b); -1.27V (c) and -1.24V (d), respectively, on TiO<sub>2</sub> (I). And FESEM images of CdSe deposited potentiostatically on TiO<sub>2</sub> (II) for 100s (e) for 200s at -1.33V on TiO<sub>2</sub> (II) (f). EDS results are also illustrated in (g) corresponding to above (a) CdSe/TiO<sub>2</sub> (I) and (f) CdSe/TiO<sub>2</sub> (II), respectively

vacancy effect on anatase TiO<sub>2</sub> (101) electronic properties, which favors the presence of states generated within the energy gap of anatase. Thus the oxygen vacancies induces more Ti<sup>3+</sup> species with localized electronic states. These Ti<sup>3+</sup> species can promote the electrical conductivity. Some of these localized inter-gap states are likely to mix with those at the bottom of the conduction band. Thus, the effective energy gap shrinks, increasing the charge carrier number. Based on calculations of Rubio-Ponce *et al.*<sup>35</sup> the surface Ti<sup>3+</sup> species presence in (101) face of anatase TiO<sub>2</sub> drastically improves its photocatalytic

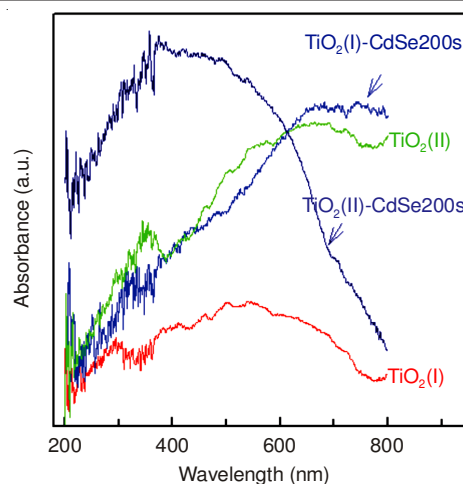


Fig. 4. UV-visible absorbance spectra of TiO<sub>2</sub> (I) (synthesized for 6 h at 200 °C) (a); CdSe-TiO<sub>2</sub> (I) for 200s-1.33V-deposition (b); TiO<sub>2</sub> (II) (synthesized for 12 h at 200 °C) (c); CdSe-TiO<sub>2</sub> (II) for 200s at -1.33V on TiO<sub>2</sub> (II) (d)

properties. Here the key point is that the strong mixing of QD and TiO<sub>2</sub> electronic levels necessitates successful electron transfer between them, suppressing the harmful influence of oxygen vacancy-Ti<sup>3+</sup> functioning as recombination centers<sup>29</sup>. In our case, the waves of CdSe and TiO<sub>2</sub> electronic levels indicated no discrete absorbance bands of CdSe and TiO<sub>2</sub> (II) nanoclusters but only a union band favorable for electron transfer between them.

The photoresponse measurements results at bias of 0.0 V (*vs.* SCE)) of the CdSe-TiO<sub>2</sub> (I) and (II) were shown in Fig. 5 (-1.33 V deposition for 200 s CdSe-TiO<sub>2</sub> (I), under illumination of visible (a) and white sunlight (b), -1.33V-deposition 200s CdSe-TiO<sub>2</sub> (II) under illumination of visible (c) and white sunlight (d)). The J-t (photocurrent density-time) curves were obtained using a photoelectrochemical cell containing CdSe/TiO<sub>2</sub> as the photoanode and Pt as the counter electrode at a constant potential of 0.0 V (*vs.* SCE). In terms of photoresponse, TiO<sub>2</sub> (II) series overwhelms TiO<sub>2</sub> (I) series, firstly, the photocurrent of TiO<sub>2</sub> (II) series suddenly rises to the maximum upon illumination turn-on and decreases to zero as soon as turn-off. In the reference group, however, TiO<sub>2</sub> (I) series is slow in both photocurrent rising and falling. It is well known that charge carriers have longer lifetime in single crystal than in polycrystal, longer lifetime means smaller transportation resistance, hence smaller response time upon external excitation- on and off of illumination. In this case, the single crystals vertical to substrate should attract electrons more directly due to the almost uniform [001] orientation and more powerfully drive into Ti electrode due to the ohmic contact between TiO<sub>2</sub> and Ti. When a closer interface between CdSe and TiO<sub>2</sub> (II) is constructed *via* 2-amino-3-sulfhydrylpropanoic acid, the quasi coaxial hierarchy structure ensures the rapid transfer of the carriers, enabling rapid photocurrent.

Secondly, the current density in CdSe-TiO<sub>2</sub> (II) achieves 0.8 and 1.3 mA cm<sup>-2</sup> without and with CdSe, respectively, but only 0.1 and 0.15 mA cm<sup>-2</sup>, in that of CdSe-TiO<sub>2</sub> (I). Herein quasi single crystal demonstrates a nearly ten times increase of photocurrent density. The well-formed 1D quasi single crystalline conductor offers electrons shortcuts to Ti substrate,

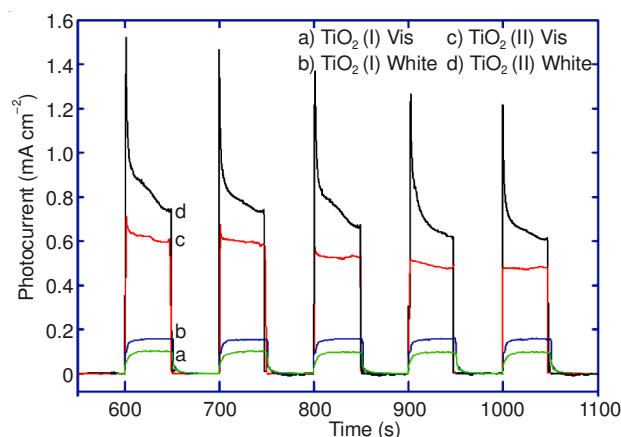


Fig. 5. Photocurrent response to on-off cycles of illumination for -1.33 V deposition for 200s CdSe-TiO<sub>2</sub> (I), under illumination of visible lights (a) and white sunlight (b); -1.33 V-deposition 200s CdSe-TiO<sub>2</sub> (II) under illumination of visible lights (c) and white sunlight (d)

demonstrating superiority compared with any other percolate paths formed by particles.

Based on the fact that visible accounts for about 65 % of response current of the white sunlight for both TiO<sub>2</sub> (II) and (I), it is suggestive that CdSe enhances the TiO<sub>2</sub> response to sunlight by enhancement of visible light harvest (Fig. 4) and conversion. We assume CdSe performs synergistically with TiO<sub>2</sub>, thus simultaneous excitation of these two heterojunctional phases promotes the electron transfer between them.

A key role of the bifunctional 2-amino-3-sulfhydryl-propanoic acid molecule is linking the acceptor and donor materials, with its carboxylic group preferential binding Ti atoms in TiO<sub>2</sub>, on the other hand its thiol (-SH) group is a desirable ligand to bind to metal chalcogenide QDs such as CdSe<sup>36,37</sup>. The chemical bond strengthened interface greatly facilitate electrons transfer from CdSe to heterojunctional TiO<sub>2</sub>. Rough and deeply gullied as the surface of TiO<sub>2</sub> (II), it is difficult to induce CdSe deep to the roots of TiO<sub>2</sub> nanospillars, without the precedent modification of bifunctional 2-amino-3-sulfhydrylpropanoic acid there were not successful CdSe deposition in our experiments. So that the virtue of strong visible-range absorption of single crystal TiO<sub>2</sub> nanoclusters were fully developed by CdSe alliance, the electrode exhibits excellent photoresponse in photoelectrochemical cells to visible lights, whose contribution is significant compared with that of ultraviolet lights.

Fig. 6 shows photocurrent density-potential (*vs.* SCE) of -1.33V-deposition CdSe for 100s (a) and 200s (b) on TiO<sub>2</sub> (II) under natural day lights scattered indoor, UV, visible, white sunlight, respectively, at scanning rate of 20 mV s<sup>-1</sup>. For CdSe/TiO<sub>2</sub>(II) 100s (a), when compared with natural light, the ultraviolet increases photocurrent more than the visible, the white light increase almost the sum of their respective increments. It is interesting to note that although the visible improves the photocurrent density, the V<sub>OC</sub> decreases simultaneously. This might be due to the lack of activation of TiO<sub>2</sub> photocatalysis by ultraviolet, revealing difficulty for TiO<sub>2</sub> in accepting the electrons from CdSe as well as transporting them<sup>24</sup>. This is an evidence of CdSe sensitizing TiO<sub>2</sub> in the visible light.

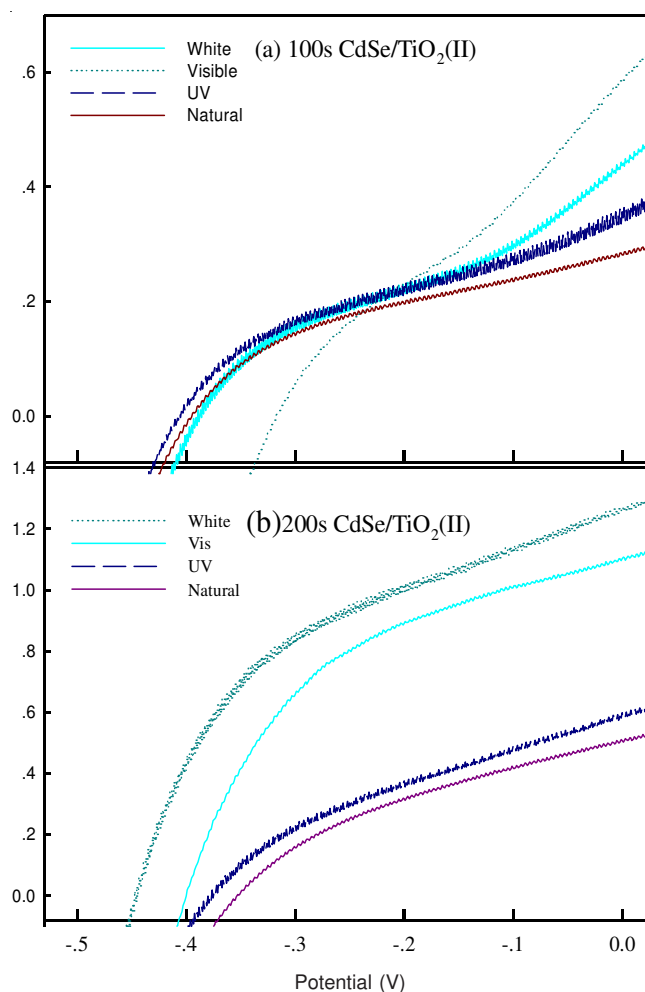


Fig. 6. Photocurrent density *versus* applied electrode potential (*vs.* SCE) of -1.33 V-deposition CdSe for 100s (a) and 200s (b) on TiO<sub>2</sub> (II) under natural day lights scattered indoor, UV, visible, white sunlight, respectively, at scanning rate of 20 mV s<sup>-1</sup>

In Fig. 6(b) J<sub>SC</sub> and V<sub>OC</sub> both increase to a modest extent. Relative to the natural light, the photocurrent dramatically increases in visible while V<sub>OC</sub> increases less. Combination of the UV and the visible leads to a synergy effect for simultaneous photocurrent and V<sub>OC</sub> increase. That is to say the electrons from CdSe excitation and separation are fully transferred to TiO<sub>2</sub>. An apparent difference between Fig. 6(b) and (a) is that the photocurrent density and V<sub>OC</sub> both surge under visible light illumination, due to improved absorption of visible light caused by improved coverage of CdSe. Meanwhile, the improved coverage of CdSe effectively hinders electrons entering into TiO<sub>2</sub> to recombine with oxidized species in the electrolyte solution.

The increase of photocurrent density under visible light illumination is larger than that under ultraviolet lights illumination and dual illumination would cause almost the sum of their respective increased photocurrent density (Fig. 6). With adequate CdSe coating, visible and UV photons have similar conversion efficiency. However, with inadequate CdSe, the visible light illumination improves the photocurrent density while decreases V<sub>OC</sub>, which is due to increased impedance against electrons in the lack of ultraviolet activation of TiO<sub>2</sub> photocatalysis.

## Conclusion

Vertically oriented single-crystal anatase TiO<sub>2</sub> nanoclusters were hydrothermally synthesized on Ti substrate in TMAOH solution at 200 °C for 12 h, CdSe from selenosulfite solution was electrodeposited down to TiO<sub>2</sub> nanoclusters roots via precedent immersion in by 2-amino-3-sulfhydrylpropanoic acid. The UV-visible absorbance spectra show the incorporation of CdSe in TiO<sub>2</sub> increases significantly absorption of visible light. More importantly, the visible and ultraviolet absorption bands have merged into a union, suggesting a mixing of their energy levels. CdSe-TiO<sub>2</sub> demonstrates visible responses superior over UV to on-off illumination in photoelectrochemical cells. Compared to natural light, 100s-CdSe-TiO<sub>2</sub> has surge photocurrent to visible illumination at the cost of the open circuit voltage, presumably because of the lack of full activation of TiO<sub>2</sub> by ultraviolet, but 200s-CdSe-TiO<sub>2</sub> has gained stable increase in both photocurrent and V<sub>oc</sub>.

## ACKNOWLEDGEMENTS

This research was supported by the National Natural Science Foundation of China (Nos. 11174227, 51209023, J1210061, 61166005), the Hubei Province Science and Technology Support Project (No. 2013BHE012) and the Fundamental Research Funds for the Central Universities.

## REFERENCES

- M.D. McGehee, *Mater. Res. Soc. Bull.*, **34**, 95 (2009).
- H. Hoppe and N.S. Saricifci, *Adv. Polym. Sci.*, **214**, 1 (2008).
- Z. Fan, D.J. Ruebusch, A.A. Rathore, R. Kapadia, O. Ergen, P.W. Leu and A. Javey, *Nano Res.*, **2**, 829 (2009).
- X. Fan, M. Zhang, X. Wang, F. Yang and X. Meng, *J. Mater. Chem. A*, **1**, 8694 (2013).
- H.B. Wu, H.H. Hng and X.W. Lou, *Adv. Mater.*, **24**, 2567 (2012).
- B. O'Regan and M. Grätzel, *Nature*, **353**, 737 (1991).
- M. Grätzel, *Nature*, **414**, 338 (2001).
- J. Luo, L. Ma, T. He, C.F. Ng, S. Wang, H. Sun and H.J. Fan, *J. Phys. Chem. C*, **116**, 11956 (2012).
- W.X. Guo, C. Xu, X. Wang, S.H. Wang, C.F. Pan, C.J. Lin and Z.L. Wang, *J. Am. Chem. Soc.*, **134**, 4437 (2012).
- G.H. Tian, Y.J. Chen, H.L. Bao, X.Y. Meng, K. Pan, W. Zhou, C.G. Tian, J.Q. Wang and H.G. Fu, *J. Mater. Chem.*, **22**, 2081 (2012).
- K. Shankar, G.K. Mor, M. Paulose, O.K. Varghese and C.A. Grimes, *J. Non-Cryst. Solids*, **354**, 2767 (2008).
- J.Y. Kim, D. Lee, H.J. Kim, I. Lim, W.I. Lee and D.-J. Jang, *J. Mater. Chem. A*, **1**, 5982 (2013).
- S.C. Hou, X. Cai, H.W. Wu, Z.B. Lv, D. Wang, Y.P. Fu and D.C. Zou, *J. Power Sources*, **215**, 164 (2012).
- Z. Zhou, J. Fan, X. Wang, W. Zhou, Z. Du and S. Wu, *Mater. Interfaces*, **3**, 4349 (2011).
- B. Liu and E.S. Aydil, *J. Am. Chem. Soc.*, **131**, 3985 (2009).
- X.J. Feng, K. Shankar, O.K. Varghese, M. Paulose, T.J. Latempa and C.A. Grimes, *Synth. Details Applications Nano Lett.*, **8**, 3781 (2008).
- B. Liu, A. Khare and E.S. Aydil, *Chem. Commun. (Camb.)*, **48**, 8565 (2012).
- B. Liu and E.S. Aydil, *J. Am. Chem. Soc.*, **131**, 3985 (2009).
- D.P. Shepherd, J.B. Sambur, Y.Q. Liang, B.A. Parkinson and A. Van Orden, *J. Phys. Chem. C*, **116**, 21069 (2012).
- J.B. Sambur, S.C. Riha, D.J. Choi and B.A. Parkinson, *Langmuir*, **26**, 4839 (2010).
- G. Tian, K. Pan, Y. Chen, J. Zhou, X. Miao, W. Zhou, R. Wang and H. Fu, *J. Power Sources*, **238**, 350 (2013).
- J.B. Sambur and B.A. Parkinson, *J. Am. Chem. Soc.*, **132**, 2130 (2010).
- Y.R. Smith, R.S. Ray, K. Carlson, B. Sarma and M. Misra, *Materials*, **6**, 2892 (2013).
- Y. Bu, Z. Chen, W. Li and J. Yu, *ACS Appl. Mater. Interfaces*, **5**, 5097 (2013).
- B.R. Hyun, A.C. Bartnik, L. Sun, T. Hanrath and F.W. Wise, *Nano Lett.*, **11**, 2126 (2011).
- A.J. Nozik, *Nano Lett.*, **10**, 2735 (2010).
- M.C. Hanna and A.J. Nozik, *J. Appl. Phys.*, **100**, 074510 (2006).
- R.D. Schaller, M.A. Petruska and V.I. Klimov, *Appl. Phys. Lett.*, **87**, 253102 (2005).
- Y. Yang, W. Rodríguez-Córdoba, X. Xiang and T. Lian, *Nano Lett.*, **12**, 303 (2012).
- H. Zhang and J.F. Banfield, *J. Mater. Chem.*, **8**, 2073 (1998).
- X. Dong, J. Tao, Y. Li and H. Zhu, *Appl. Surf. Sci.*, **256**, 2532 (2010).
- J. Wu, T. Zhang, Y. Zeng, S. Hayakawa, T. Kanji and A. Osaka, *Langmuir*, **21**, 6995 (2005).
- Y. Chen, X. He, X. Zhao, Q. Yuan and X. Gu, *J. Colloid Interf. Sci.*, **310**, 171 (2007).
- W.Q. Fang, J.Z. Zhou, J. Liu, Z.G. Chen, C. Yang, C.H. Sun, G.R. Qian, J. Zou, S.Z. Qiao and H.G. Yang, *Chem. Eur. J.*, **17**, 1423 (2011).
- N.S. Portillo-Vélez, O. Olvera-Neria, I. Hernández-Pérez and A. Rubio-Ponce, *Surf. Sci.*, **616**, 115 (2013).
- R.S. Selinsky, Q. Ding, M.S. Faber, J.C. Wright and S. Jin, *Chem. Soc. Rev.*, **42**, 2963 (2013).
- L. Li, X.C. Yang, J.J. Gao, H.N. Tian, J.Z. Zhao, A. Hagfeldt and L.C. Sun, *J. Am. Chem. Soc.*, **133**, 8458 (2011).